J|A|C|S
ARTICLES
Published on Web 08/29/2006

Synthesis, Structural Studies, Theoretical Calculations, and Linear and Nonlinear Optical Properties of Terpyridyl Lanthanide Complexes: New Evidence for the Contribution of f Electrons to the NLO Activity

Katell Sénéchal-David,[†] Anne Hemeryck,[‡] Nicolas Tancrez,[§] Loïc Toupet,[⊥] J. A. Gareth Williams,[∥] Isabelle Ledoux,[§] Joseph Zyss,[§] Abdou Boucekkine,[‡] Jean-Paul Guégan,[†] Hubert Le Bozec,*[,†] and Olivier Maury*[,†,▽]

Contribution from the Laboratoire de Chimie de Coordination et Catalyse, UMR 6509 CNRS−Université Rennes 1, Institut de Chimie, Campus de Beaulieu, 35042 Rennes Cedex, France, Laboratoire de Chimie du Solide et Inorganique Moléculaire, UMR 6511 CNRS−Université Rennes 1, Institut de Chimie, Campus de Beaulieu, 35042 Rennes Cedex, France, Groupe de la Matière Condensée et Matériau, UMR 6626 CNRS−Université de Rennes 1, Campus de Beaulieu, 35042 Rennes Cedex, France, Department of Chemistry, University of Durham, South Road, Durham DH1 3LE, U.K., and Laboratoire de Physique Quantique Moléculaire, ENS Cachan, 61 avenue du président Wilson, 94235 Cachan, France

Received June 1, 2006; E-mail: olivier.maury@ens-lyon.fr

Abstract: The synthesis and structural, photophysical, and second-order nonlinear optical (NLO) properties of a novel lanthanide terpyridyl-like complex family **L**Ln$(NO_3)_3$ (Ln = La, Gd, Dy, Yb, and Y) are reported. The isostructural character of this series in solution and in the solid state has been established on the basis of X-ray diffraction analysis in the cases of yttrium and gadolinium complexes, theoretical optimization of geometry (DFT), and NMR spectroscopy. The absorption, emission, and solvatochromic properties of the free terpyridyl-like ligand **L** were thourougly investigated, and the twist intramolecular charge transfer (TICT) character of the lowest energy transition was confirmed by theoretical calculation (TDDFT and CIS). The similar ionochromic effect of the different lanthanide ions was evidenced by the similar UV−visible spectra of the complete family of complexes. On the other hand, the quadratic hyperpolarizability coefficient β, measured by the harmonic light scattering (HLS) technique, is clearly dependent on the nature of the metal, and a careful examination of the particular case of yttrium unambiguously confirms the contribution of metal f electrons to the NLO activity.

Introduction

Since the pioneering work of Frasier[1] and Green,[2] organometallic and coordination complexes have been widely studied for the design of chromophores for second-order nonlinear optics (NLO).[3] At the end of the 1980s, organotransition metal complexes generally presented low NLO activity and were mainly academic curiosities, but at present such compounds have become increasingly important for the design of highly active multidimensional dipolar[4] and octupolar[5] NLO-phores. Moreover, due to the intrinsic properties of transition metals, such as the large number of stable oxidation states or the presence of unpaired electrons, metallo-chromophores are very promising for the design of molecular NLO switches[3g,6,7] and multifunctional materials combining NLO and magnetic properties, for example.[8,7e] However, despite the large number of studies reported in the literature, a better rationalization of the role of

[†] Laboratoire de Chimie de Coordination et Catalyse, Université Rennes 1.
[‡] Laboratoire de Chimie du Solide et Inorganique Moléculaire, Université Rennes 1.
[§] ENS Cachan.
[⊥] Groupe de la Matière Condensée et Matériau, Université Rennes 1.
[∥] University of Durham.
[▽] Current adress: Laboratoire de Chimie, UMR 5182 ENS-Lyon, 46 Allée d'Italie, F-69364 Lyon Cedex 07, France.

(1) Frasier, C. C.; Harvey, M. A.; Cokerham, M. P.; Hand, H. M.; Chauchard, E. A.; Lee, C. H. *J. Phys. Chem.* **1986**, *90*, 5703−5706.
(2) Green, M. L. H.; Marder, S. R.; Thompson, M. E.; Bandy, J. A.; Bloor, D.; Kolinsky, P. V.; Jones, R. J. *Nature* **1987**, *330*, 360−362.
(3) (a) Long, N. J. *Angew. Chem., Int. Ed. Engl.* **1995**, *34*, 21−38. (b) Whittall, I. R.; McDonagh, A. M.; Humphrey, M. G.; Samoc, M. *Adv. Organomet. Chem.* **1998**, *42*, 291−362; **1999**, *43*, 349−405. (c) Lacroix, P. G. *Eur. J. Inorg. Chem.* **2001**, 339−348. (d) Renouar, T.; Le Bozec, H. *Eur. J. Inorg. Chem.* **2001**, 229−239. (e) Di Bella, S. *Chem. Soc. Rev.* **2001**, *30*, 355−366. (f) Coe, B. J. In *Comprehensive Coordination Chemistry II*; McCleverty, J. A., Meyer, T. J., Eds.; Elsevier Pergamon: Oxford U.K., 2004; Vol 9, pp 621−687. (g) Powell, C. E.; Humphrey, M. G. *Coord. Chem. Rev.* **2004**, *248*, 725−756. (h) Maury, O.; Le Bozec, H. *Acc. Chem. Res.* **2005**, *38*, 691−704.
(4) (a) Le Cours, S. M.; Guan, H.-W.; DiMagno, S. G.; Wang, C. H.; Therien, M. J. *J. Am. Chem. Soc.* **1996**, *118*, 1497−1503. (b) Zhang, T.-G.; Zhao, Y.; Asselberg, I.; Persoons, A.; Clays, K.; Therien, M. J. *J. Am. Chem. Soc.* **2005**, *127*, 9710−9720. (c) Alain, V.; Blanchard-Desce, M.; Chen, C.-T.; Marder, S. R.; Fort, A.; Barzoukas, M. *Synth. Met.* **1996**, *81*, 133−136. (d) Liao, Y.; Eichinger, B. E.; Firestone, K. A.; Haller, M.; Luo, J.; Kaminsky, W.; Benedict, J. B.; Reid, P. J.; Jen, A. K.-Y.; Dalton, L. R.; Robinson, B. H. *J. Am. Chem. Soc.* **2005**, *127*, 2758−2766.
(5) (a) Maury, O.; Viau, L.; Sénéchal, K.; Corre, B.; Guégan, J.-P.; Renouard, T.; Ledoux, I.; Zyss, J.; Le Bozec, H. *Chem.−Eur. J.* **2004**, *10*, 4454−4466. (b) Viau, L.; Bidault, S.; Maury, O.; Brasselet, S.; Ledoux, I.; Zyss, J.; Ishow, E.; Nakatani, K.; Le Bozec, H. *J. Am. Chem. Soc.* **2004**, *126*, 8386−8387.

Scheme 1 [a]

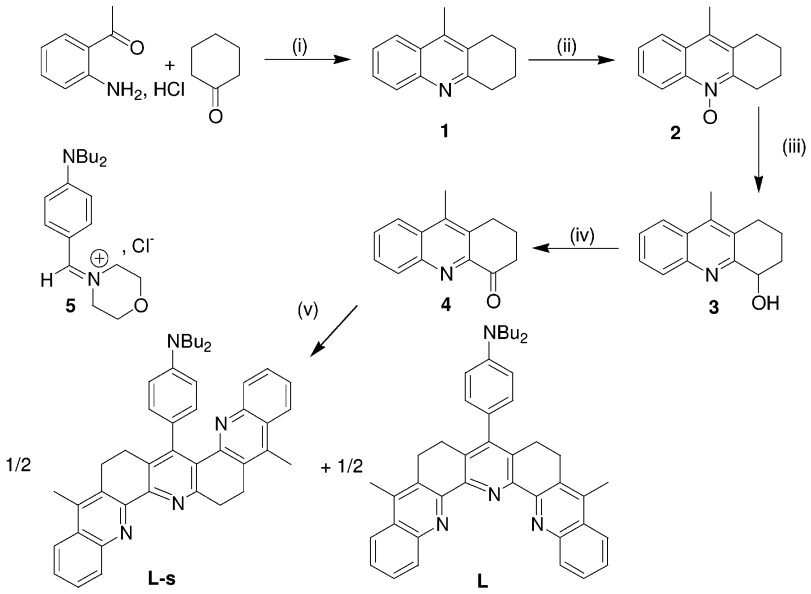

[a] (i) Solvent-free, 115 °C, 18 h, 90%; (ii) *m*-CPBA, CH_2Cl_2, RT, 3 h, 99%; (iii) $(TfO)_2O$, CH_2Cl_2, RT, 2 h, 30 min, directly followed by K_2CO_3, MeOH, RT, 3 h, 87%; (iv) MnO_2, CH_2Cl_2, RT, 3 days, 58% after column chromatography; (v) (a) $CHCl_3$, reflux, NH_4OAc, 18 h; (b) NH_3 (25% in water), RT, 4 h, 42% after column chromatography.

the metal in the global NLO activity of the chromophore is still lacking. Transition metals can act (i) as purely donor end groups, as in the case of metallocenes[2,4c,4d] or metal acetylides[9] or (ii) as purely inductive acceptor groups enforcing the intraligand charge-transfer character (ILCT).[10] In most cases, *d* orbitals are involved in many different low-energy optical charge-transfer transitions like metal-to-ligand (MLCT), ligand-to-metal (LMCT), metal-centered (MC), intervalence (IVCT), or more complex ligand-to-metal-to-ligand (LMLCT) charge-transfer transitions. The overall NLO activity of the complex results from the contributions of the transitions centered on both the metal and the ligands (ILCT). These charge transfers are generally multidirectionnal, so it is very difficult to dissociate and quantify the various contributions and clearly define the role of the metal.[3c−e,5a,10d,11]

It is worth noting that all the studies on metal-containing chromophores have been carried out with transition metals, and almost nothing is known about the potential of lanthanide complexes in second-order NLO.[12] This is very surprising because the very strong chemical similarities of the lanthanide(III) ions (La−Lu) offer a unique opportunity to design an isostructural series in which only intraligand charge-transfer transitions occur. These reasons prompted us to undertake the design of dipolar and octupolar lanthanide complexes in order to study the influence of the metal on the second-order NLO activity. Furthermore, we recently established, for the first time, a clear correlation between the quadratic hyperpolarizabilities, β, and the electronic f configuration of the rare earth in octupolar $Ln(DPA)_3,3Na\cdot xH_2O$ complexes (DPA = 2,6-pyridinedicarboxylate).[13] To confirm the contribution of f electrons to β, we decided to prepare a second dipolar series based on a functionalized annelated terpyridine ligand exibiting a higher NLO activitity.[14] In this paper are described the syntheses of the ligand and the related lanthanide complexes (Ln = La, Dy, Gd, Yb and Y); the isostructural character of the familly was established by means of solution, structural, and theoretical geometry optimization studies. The photophysical properties (absorption and luminescence) were carefully investigated and interpreted using theoretical calculations. Finally the second-order NLO properties were measured by harmonic light scattering (HLS) techniques, unambiguously confirming the contribution of metal f electrons to the complex quadratic hyperpolarizability.

(6) For a review see: Coe, B. J. *Chem.−Eur. J.* **1999**, *5*, 2464−2471.
(7) (a) Coe, B. J.; Houbrechts, S.; Asselberghs, I.; Persoons, A. *Angew. Chem., Int. Ed.* **1999**, *38*, 366−368. (b) Weyland, T.; Ledoux, I.; Brasselet, S.; Zyss, J.; Lapinte, C. *Organometallics* **2000**, *19*, 5235−5237. (c) Malaun, M.; Reeves, Z. R.; Paul, R. L.; Jeffery, J. C.; McCleverty, J. A.; Ward, M. D.; Asselberghs, I.; Clays; K.; Persoons, A. *Chem. Commun.* **2001**, 49−50. (d) Asselberghs, I.; Clays, K.; Persoons, A.; McDonagh, A. M.; Ward, M. D.; McCleverty, J. A. *Chem. Phys. Lett.* **2002**, *368*, 408−411. (e) Sporer, C.; Ratera, I.; Ruiz-Molina, D.; Zhao, Y.; Vidal-Gancedo, J.; Wurst, K.; Jaitner, P.; Clays, K.; Persoons, A.; Rovira, C.; Veciana, J. *Angew. Chem., Int. Ed.* **2004**, *43*, 5266−5268.
(8) (a) Lacroix, P. G. *Chem. Mater.* **2001**, *13*, 3495−3506. (b) Margeat, O.; Lacroix, P. G.; Costes, J.-P.; Donnadieu, B.; Lepetit, C.; Nakatani, K. *Inorg. Chem.* **2004**, *43*, 4743−4750.
(9) For an exhaustive review, see ref 3g and references therein.
(10) (a) Bourgault, M.; Baum, K.; Le Bozec, H.; Pucetti, G.; Ledoux, I.; Zyss, J. *New J. Chem.* **1998**, 517−522. (b) Roberto, D.; Ugo, R.; Bruni, S.; Cariati, E.; Cariati, F.; Fantucci, P. C.; Invernizzi, I.; Quici, S.; Ledoux, I.; Zyss, J. *Organometallics* **2000**, *19*, 1775−1788. (c) Roberto, D.; Ugo, R.; Tessore, F.; Lucenti, E.; Quici, S.; Vezza, S.; Fantucci, P. C.; Invernizzi, I.; Bruni, S.; Ledoux-Rak, I.; Zyss, J. *Organometallics* **2002**, *21*, 161−170. (d) Sénéchal, K.; Maury, O.; Le Bozec, H.; Ledoux, I.; Zyss, J. *J. Am. Chem. Soc.* **2002**, *124*, 4561−4562. (e) Tessore, F.; Roberto, D.; Ugo, R.; Mussini, P.; Quici, S.; Ledoux-Rak, I.; Zyss, J. *Angew. Chem., Int. Ed.* **2003**, *42*, 456−459.
(11) (a) Kanis, D. R.; Lacroix, P. G.; Ratner, M. A.; Marks, T. J. *J. Am. Chem. Soc.* **1994**, *116*, 10089−10102. (b) Cummings, S. D.; Cheng, L.-T.; Eisenberg, R. *Chem. Mater.* **1997**, *9*, 440−450. (c) Vance, F. W.; Hupp, J. T. *J. Am. Chem. Soc.* **1999**, *121*, 4047−4053. (d) Gaudry, J. B.; Capes, L.; Langot, P.; Marcen, S.; Kollmansberger, M.; Lavastre, O.; Freysz, E.; Letard, J.-F.; Kahn, O. *Chem. Phys. Lett.* **2000**, *324*, 321−329. (e) Fave, C.; Hissler, M.; Sénéchal, K.; Ledoux, I.; Zyss, J.; Réau, R. *Chem. Commun.* **2002**, 1674−1675. (f) Coe, B. J.; Harris, J. A.; Brunschwig, B. S.; Asselberghs, I.; Clays, K.; Garin, J.; Orduna, J. *J. Am. Chem. Soc.* **2005**, *127*, 13399−13410. (g) Tessore, F.; Roberto, D.; Ugo, R.; Pizzotti, M.; Quici, S.; Cavazzini, M.; Bruni, S.; De Angelis, F. *Inorg. Chem.* **2005**, *44*, 8967−8978.
(12) Only the Kurtz power NLO activity of a europium-containing coordination polymer was described in: Shi, J.-M.; Xu, W.; Liu, Q.-Y.; Liu, F.-L.; Huang, Z.-L.; Lei, H.; Yu, W.-T.; Fang, Q. *Chem. Commun.* **2002**, 756−757.
(13) Tancrez, N.; Feuvrie, C.; Ledoux, I.; Zyss, J.; Toupet, L.; Le Bozec, H.; Maury, O. *J. Am. Chem. Soc.* **2005**, *127*, 13474−13475.
(14) A part of this study has been preliminarily published in: Sénéchal, K.; Toupet, L.; Ledoux, I.; Zyss, J.; Le Bozec, H.; Maury, O. *Chem. Commun.* **2004**, 2180−2181.

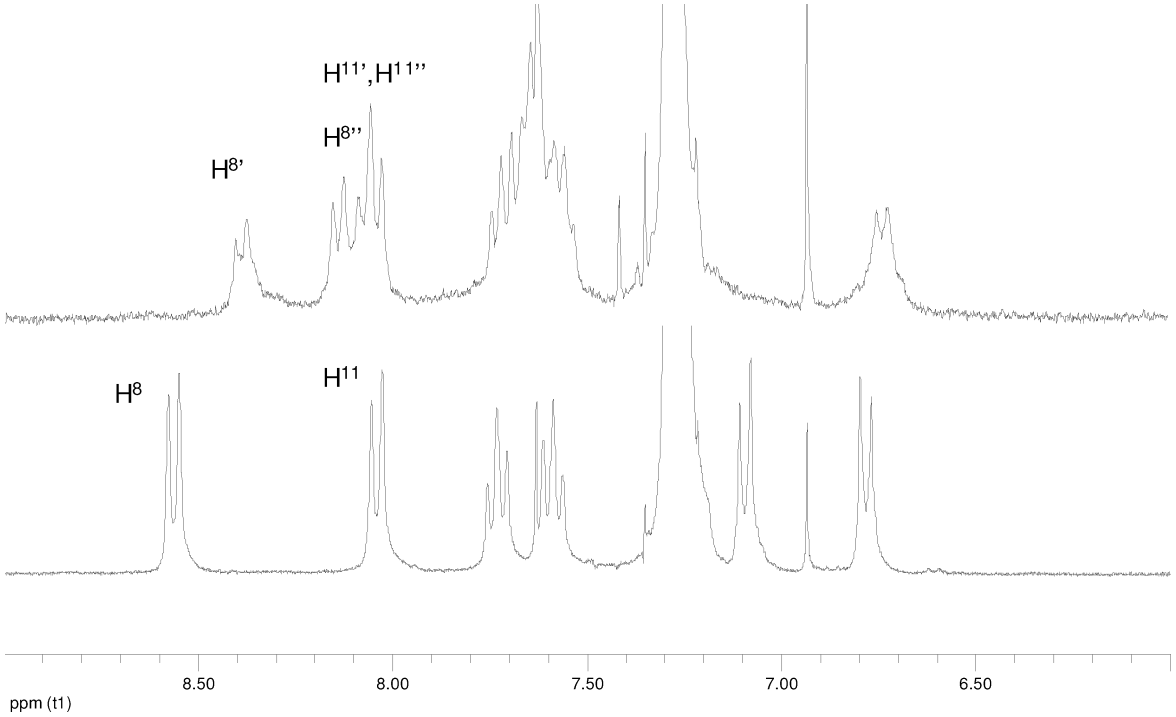

Figure 1. Comparison of the aromatic region of the ^{1}H NMR spectra ($CDCl_3$, 500 MHz, RT) of **L-s** (top) and **L** (bottom).

Scheme 2. Protonation of **L** To Generate the Cation **L**H$^+$ and Its Isolation as the Triflate Salt

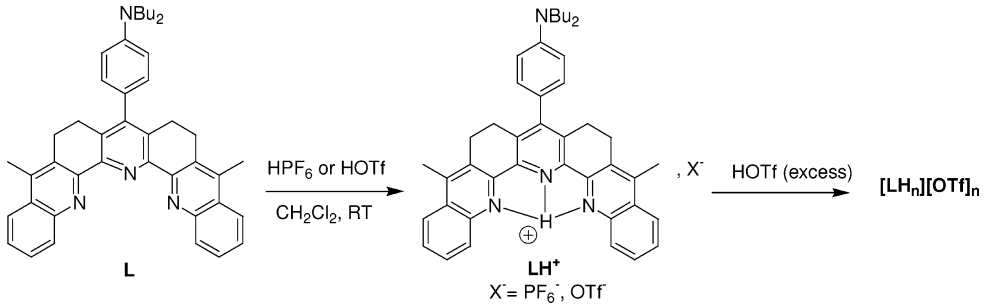

Results and Discussion

Ligand Synthesis and Protonation Reaction. The target ligand **L** (Scheme 1) is a rigidified terpyridine-like ligand whose central pyridinic ring is functionalized by a *p*-dibutylaminophenyl moiety in order to induce an intraligand charge-transfer transition from the amino donor to the pyridine acceptor group. The ligand features also a dimethylene annelation between the central pyridinic ring and the distal quinoline moieties in order to force a *cisoid* conformation, stabilizing its rare-earth complexes against competitive coordination of solvent.[15] Generally, annelated terpyridine can be prepared either from morpholine enamines derived from α-pyridyl ketones and aldehydes[16] or from α-pyridyl ketones and the corresponding iminium salts.[17] The ligand **L** was prepared in 32% overall yield by employing the second synthetic procedure described by Rish and coworkers (Scheme 1).[17] The acridine **1** was obtained by a Friedländer condensation between *o*-aminoacetophenone hydrochloride and cyclohexanone. The ketone **4** was synthesized by a three-step procedure: (a) N-oxidation of **1**, (b) Boekelheide rearrangement, and (iii) oxidation of the resulting alcohol. Finally, reaction between the iminium chloride **5**[18] and 2 equiv of **4** in basic media, followed by cyclization in the presence of ammonia afforded a 1/1 mixture of *U*- and *S*-shape annelated terpyridine isomers **L** and **L-s**, which could be separated by column chromatography.[19] Experimental details and characterization by NMR, elemental analysis, and high-resolution mass spectrometry are described in the Experimental Section. The isomers can be easily distinguished by their NMR spectra (Figure 1). **L** features an overall C_2 symmetry resulting in more simple ^{1}H and ^{13}C NMR spectra than those of **L-s**. For instance, the more downfield shifted signals, corresponding to quinolyl protons H$^{8'}$ and H$^{11'}$ (see Figure 13 in Experimental Section for numbering) appear as two doublets in the case of **L** and four doublets in the case of **L-s**. Similarly, the ^{13}C NMR spectrum of **L-s** reveals 37 signals compared to 25 signals for **L**. A color change from pale yellow to violet occurred instantaneously upon protonation of **L** in dichloromethane with

(15) (a) Chapman, R. D.; Loda, R. T.; Riehl, J. P.; Schwartz, R. W. *Inorg. Chem.* **1984**, *23*, 1652−1657. (b) Mallet, C.; Thummel, R. P.; Hery, C. *Inorg. Chim. Acta* **1993**, *210*, 223−231.
(16) (a) Hegde, V.; Jahng, Y.; Thummel, R. P. *Tetrahedron Lett.* **1987**, *28*, 4023−4026. (b) For a short account, see: Thummel, R. P. *Synlett* **1992**, 1−12.
(17) Keuper, R.; Risch, N.; Flörke, U.; Haupt, H.-J. *Liebigs Ann.* **1996**, 705−715.
(18) Schroth, W.; Jahn, U.; Ströhl, D. *Chem. Ber.* **1994**, *127*, 2013−2022.
(19) Recently a regioselective synthesis leading only to the formation of the *U*-shaped isomer was reported in DMSO; see: Sielemann, D.; Winter, A.; Flörke, U.; Risch, N. *Org. Biomol. Chem.* **2004**, *2*, 863−868.

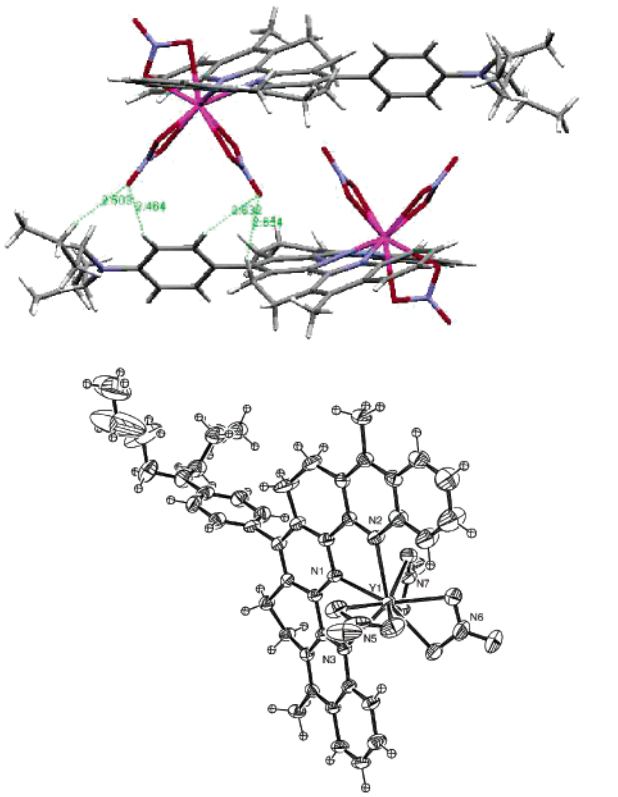

Figure 2. Head-to-tail stacking (top) and ORTEP drawing of [Y**L**$(NO_3)_3$·$^1/_2CH_3CN$·$^1/_2H_2O$] (bottom), interstitial solvent molecules being removed for clarity.

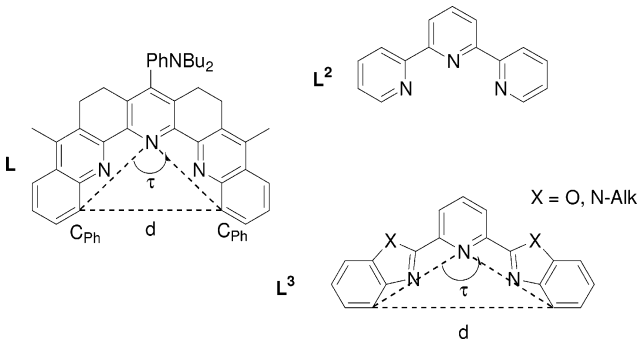

Figure 3.

Scheme 3. Preparation of the Dipolar Complexes

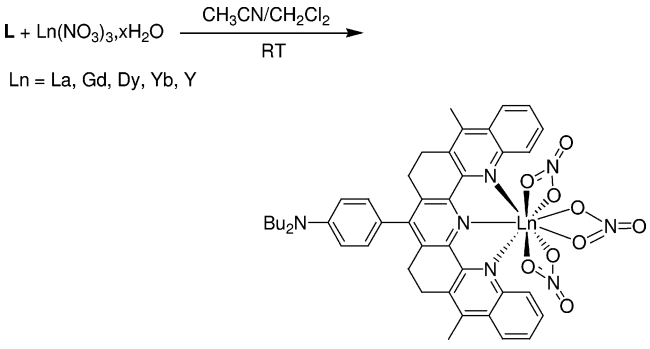

1 equiv of HPF_6, (Scheme 2). The resulting salt [**L**H]$^+$ was fully characterized by ^{1}H, ^{31}P NMR, and elemental analysis. Further addition of HPF_6 results in the complete decoloration of the solution and neutralization with $NaHCO_3$ reforms the starting material **L**.

Table 1. Selected Bond Lengths (Å) and Angles (deg)

	Gd	Y
Ln−O	2.437(7)/2.446(9)	2.369(4)/2.376(4)
	2.459(8)/2.460(9)	2.428(4)/2.431(4)
	2.485(7)/2.503(8)	2.454(4)/2.465(4)
Ln−N(central)	2.445(9)	2.365(9)
Ln−N(distal)	2.551(8)/2.573(8)	2.503(4)/2.513(4)
$C_{py}-C_{ph}$	1.516(16)	1.489(7)
H-bond (intra)	2.593/2.291	2.390/2.456
N−Ph	1.384(15)	1.381(7)
C−C (interPy)	1.499(14)/1.537(15)	1.490(6)/1.493(6)
$d = C_{Ph}-C_{Ph}$	6.829	6.682
(NCCN)	10.0/15.0	2.03/10.5
Θ	79.2	95.0
τ	87.9	86.1

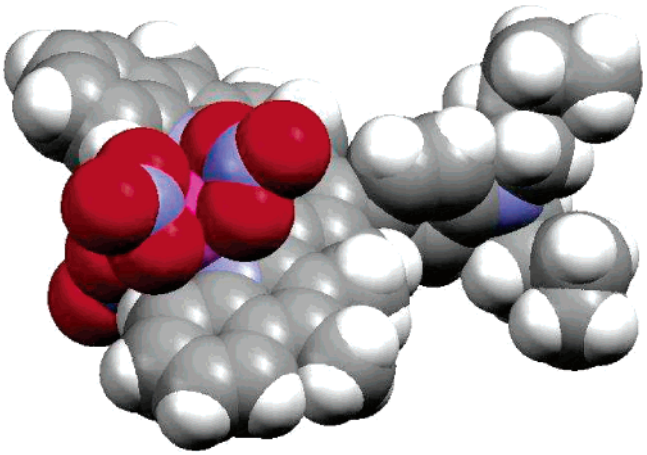

Figure 4. CPK representation of the gadolinium complex (from the crystal structure).[14]

Synthesis of Lanthanide Complexes. Treatment of ligand **L** with 1 equiv of Ln$(NO_3)_3$·xH$_2$O (x = 6 for Ln = La, Gd, and x = 5 for Dy, Yb, and Y) in dichloromethane/acetonitrile led to brown-orange Ln**L**$(NO_3)_3$ complexes in good yield (64−92%) after crystallization from hot acetonitrile and further recrystallization from a dichloromethane/pentane mixture (Scheme 3). All complexes gave satisfactory microanalysis results as dichloromethane clathrates (see Experimental Section). In the cases of gadolinium and yttrium, crystallization from acetonitrile afforded orange needle monocrystals suitable for X-ray diffraction analysis (Table S1).

Solid-State Structure of [GdL$(NO_3)_3$·CH_3CN] and [YL$(NO_3)_3$·$^1/_2CH_3CN$·$^1/_2H_2O$]. Both complexes crystallize in a centrosymmetric space group with interstitial solvent molecules. Each dipolar complex adopts a head-to-tail configuration (Figures 2 and S1), the intermolecular interactions are ensured by hydrogen bonds between noncoordinated oxygen atoms of nitrato fragments and protons belonging to the NR_2−phenyl moieties ($d_{(O\cdots H)}$ = 2.464 and 2.632 Å). In the case of yttrium, an additional interaction with the dimethylene bridge ($d_{(O\cdots H)}$ = 2.654 Å) is present. ORTEP drawings of Y (Figure 2) and Gd[14] reveal that both complexes are isostructural: the metal is nine-coordinate, being bonded to the tridentate ligand **L** and three bidentate nitrato ligands. It is worth noting that no additional solvent molecules are coordinated to the metal, acetonitrile and water being present only as interstitial compounds. This behavior is in contrast with that generally described for other Ln^{3+} complexes of terdentate nitrogen ligands such as terpyridine **L**^{2} or bis-benzimidazol-pyridine **L**^{3} (Figure 3).

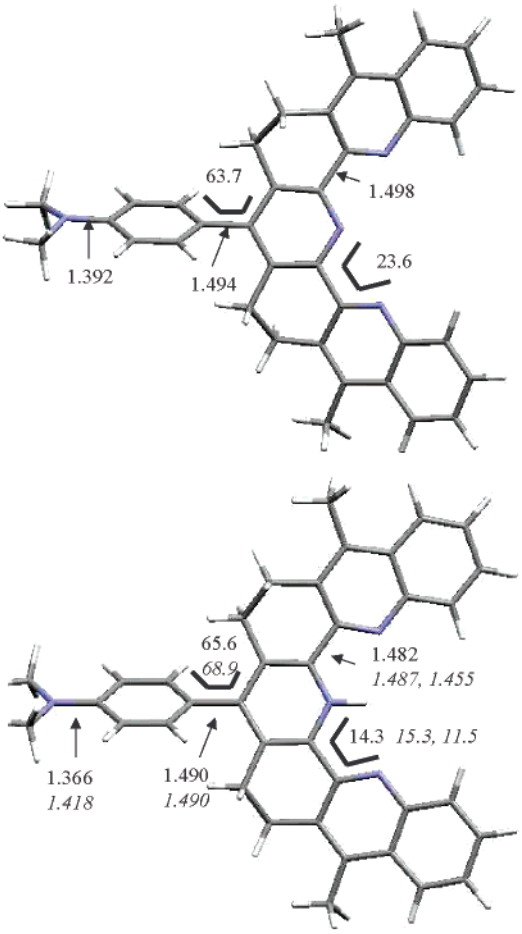

Figure 5. DF optimized geometries of **L′** (top) and **L′**H^+ (bottom), with important bond lengths (Å) and angles (deg). Experimental data are given in italics.[24]

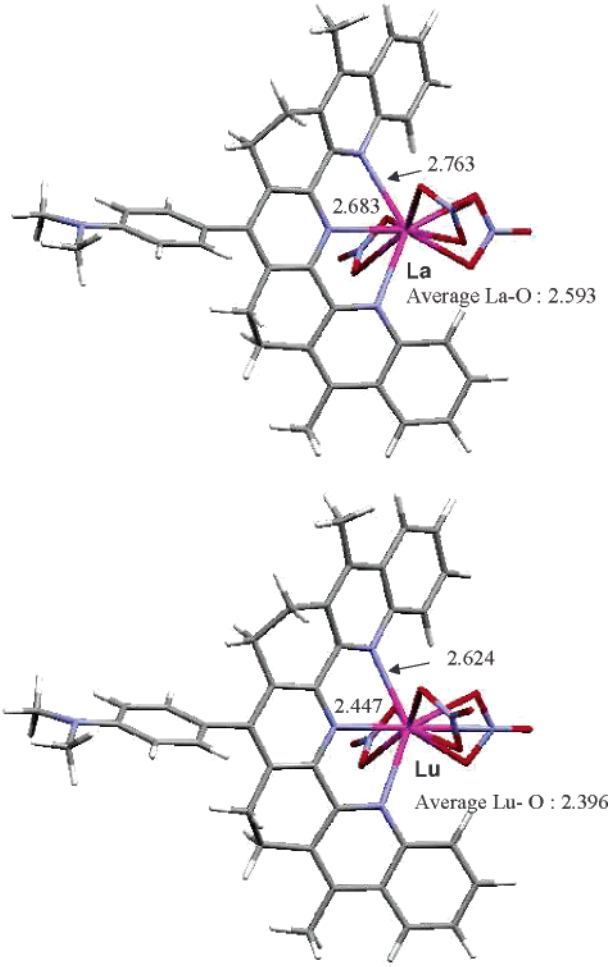

Figure 6. DF optimized geometries of the lanthanum (top) and lutetium (bottom) complexes, showing important bond lengths (Å) and angles (deg).

While the coordination number is generally 10, even 11 in the case of lanthanum, with additional coordination of water, acetonitrile, or methanol,[20,21] solvent-free nine-coordinated complexes are normally only found with ytterbium[22,20b,21b] and lutetium,[23,21b] which feature smaller ionic radius. This surprising result can be explained by the larger steric hindrance induced by **L** compared with $\mathbf{L^2}$ or $\mathbf{L^3}$: **L** presents a very rigid helicene-like structure with seven fused six-membered rings, and the replacement of a five-member imidazole ring in $\mathbf{L^2}$ by a pyridine (**L**) brings the distal phenyl ring closer to the metal. As a result, the bite angle τ ($C_{Ph}-N_{central}-C_{Ph}$, Figure 3) and the distances between the two distal phenyl rings ($d = C_{Ph}-C_{Ph}$) of the coordinated ligand are significantly smaller for $\mathbf{L}Ln(NO_3)_3$ (Y $\tau = 85°$, $d = 6.65$ Å; Gd $\tau = 87°$, $d = 6.85$ Å) than for $\mathbf{L^2}$-$Lu(NO_3)_3$ (Lu $\tau = 105°$, $d = 8.23$ Å).[21b] In consequence, to minimize the steric repulsion between the quinolinic protons and nitrato moieties, the metal is deeply embedded into the ligand cavity resulting in a smaller Ln−N distance with the central nitrogen atom than with the two distal ones (Table 1). This behavior is in marked difference with the coordination of $\mathbf{L^2}$ or $\mathbf{L^3}$, where the metal is always closer to the distal nitrogen atoms.[20−23] Therefore, the $Ln-N_{central}$ distance is significantly shorter for **L** than for $\mathbf{L^2}$ or $\mathbf{L^3}$. For example, the $Gd-N_{central}$ distance is 2.64 Å for $\mathbf{L^2}Gd(NO_3)_3(H_2O)\cdot\mathbf{L^2}$,[20e] 2.536 Å for ($\mathbf{L^2}$-$Gd(NO_3)_2(H_2O)_3)\cdot NO_3$,[20a] and only 2.495 Å for $\mathbf{L}Gd(NO_3)_3$. Thus, the absence of any coordinated solvent in both structures is clearly due to a stronger steric hindrance induced by **L**, inhibiting coordination of further molecules at the metal. The CPK representation of the gadolinium complex clearly illustrates the helicene-like structure of the ligand wrapped around the metal (Figure 4).

Solution Structure of Lanthanide Complexes. Diamagnetic (La, Y) and paramagnetic (Yb, Dy) complexes were characterized by ^1H NMR in deuterated dichloromethane, and the signals were assigned by means of COSY experiments. Only one set of signals is observed even at low temperature, indicating that

(20) For $\mathbf{L^2}$ type ligand, see: (a) Semenova, L. I.; White, A. H. *Aust. J. Chem.* **1999**, *52*, 507−517. (b) Drew, M. G. B.; Iveson, P. B.; Hudson, M. J.; Liljenzin, J. O.; Spjuth, L.; Cordier, P.-Y.; Enarson, A.;. Hill, C.; Madic, C. *Dalton Trans.* **2000**, 821−830. (c) Drew, M. G. B.; Hudson, M. J.; Iveson, P. B.; Madic, C.; Russel, M. L. *Dalton Trans.* **2000**, 2711−2720. (d) Cotton, S. A.; Noy, O. E.; Liesener, F.; Raithby, P. R. *Inorg. Chim. Acta* **2003**, *344*, 37−42. (e) Drew, M. G. B.; Hill, C.; Hudson, M. J.; Iveson, P. B.; Madic, C.; Vaillant, L.; Youngs, T. G. A. *New J. Chem.* **2004**, *28*, 462−470.

(21) For $\mathbf{L^3}$ type ligand, see: (a) Petoud, S.; Bünzli, J.-C. G.; Piguet, C. *Inorg. Chem.* **1997**, *36*, 1345−1353. (b) Terazzi, E.; Torelli, S.; Bernardinelli, G.; Rivera, J.-P.; Bénech, J.-P.; Bourgogne, C.; Donnio, B.; Guillon, D.; Imbert, D.; Bünzli, J.-C. G.; Pinto, A.; Jeannerat, D.; Piguet, C. *J. Am. Chem. Soc.* **2005**, *127*, 888−903.

(22) Ahrens, B.; Cotton, S. A.; Feeder, N.; Noy, O. E.; Raithby, P. R.; Teat, S. J. *Dalton Trans.* **2002**, 2027−2030.

(23) (a) Nozary, H.; Piguet, C.; Rivera, J.-P.; Tissot, P.; Bernardinelli, G.; Vulliermet, N.; Weber, J.; Bünzli, J.-C. G. *Inorg. Chem.* **2000**, *39*, 5286−5298. (b) Nozary, H.; Piguet, C.; Tissot, P.; Bernardinelli, G.; Bünzli, J.-C. G.; Deschenaux, R.; Guillon, D. *J. Am. Chem. Soc.* **1998**, *120*, 12274−12288.

Table 2. Selected Distances (Å) and Angles (deg) from the Optimized Geometries Obtained by DFT

	L′	L′H$^+$	L′La(NO$_3$)$_3$	L′Y(NO$_3$)$_3$	L′Lu(NO$_3$)$_3$
Ln−O			2.577/2.577	2.385/2.385	2.361/2.361
			2.598 /2.597	2.428/2.428	2.408/2.408
			2.605/2.605	2.440/2.440	2.421/2.421
Ln−N(central)			2.683	2.477	2.447
Ln−N(distal)			2.763/2.763	2.638/2.638	2.624/2.624
$C_{py}-C_{ph}$	1.494	1.490	1.499	1.499	1.499
N−Ph	1.392	1.366	1.397	1.397	1.397
C−C (interPy)	1.498/1.498	1.482/1.482	1.505/1.505	1.502/1.502	1.502/1.502
NCCN	23.6/23.6	14.3/14.3	20.7/20.7	19.5/19.5	18.8/18.8
Θ	63.7	65.6	65.1	65.5	65.9

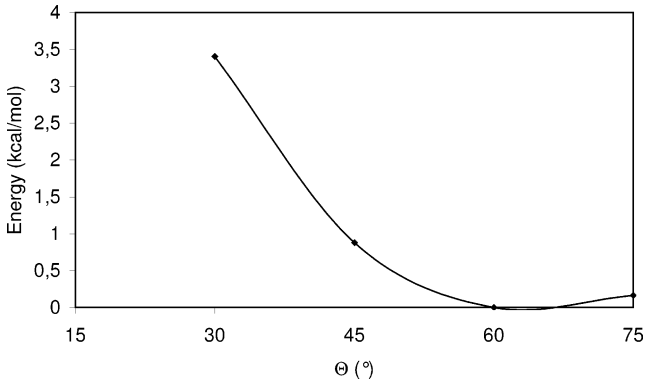

Figure 7. Plot of the energy vs θ for ligand **L′**.

the average C_2 symmetric architecture of the complexes found in the solid state is maintained in solution. For the two paramagnetic complexes studied, the ^{1}H NMR signals are spread over ca. 150 ppm and, as expected, the signals of the quinolic protons pointing toward the lanthanide ion are the most shifted ($\delta = -95.4$ ppm for Dy and $+114$ ppm for Yb). In conclusion, it appears that this family of complexes can be considered as isostructural both in the solid state and in dichloromethane solution.

DFT Calculations. A DFT study (see the Experimental Section for computational details) has been carried out on **L′** containing a NMe_2 donor group instead of NBu_2, as well as on [**L′**H]$^+$ and on the three diamagnetic complexes **L′**Ln(NO$_3$)$_3$ (Ln = Y, La, Lu). The optimized geometries (Figures 5, 6, and S2 and Table 2) are in agreement with the X-ray diffraction analysis data obtained for [**L**H]$^+$ [24] and **L**Y(NO$_3$)$_3$ (Table 1). In the case of [**L′**H]$^+$, the centrally protonated form is found to be 7.8 kcal·mol^{-1} more stable than the lateral one. The small difference from the crystal structure can be explained by the presence of a hydrogen bond with an ethanol molecule.[24] For the three lanthanide complexes, the Ln−N$_{central}$ distance is significantly shorter than the Ln−N$_{distal}$, as observed in the solid state. In addition, the dihedral angle θ between the dialkylaminophenyl and the central pyridinic ring is estimated to be around 65° versus 68°−95° in the solid state (Tables 1 and 2). However, the calculated energy variation versus θ for **L′** (Figure 7) shows a very flat minimum allowing free oscillations of θ of about 20° for a small energetic cost (<1 kcal·mol^{-1}); hence the observed differences are not really significant and can simply result from the crystal packing.

Photophysical and Nonlinear Optical Data. A. Optical Properties of L. The room-temperature absorption and emission spectra of **L** in CH_2Cl_2 are shown in Figures 8 and S3, and the data are collected in Table 3. The UV−visible absorption spectrum exhibits a broad band at 361 nm overlapped with a sharp band at 376 nm (see deconvolution). The emission spectrum exhibits a broad structureless band at 518 nm in dichloromethane with a moderate fluorescence quantum yield (0.26) and a relatively long fluorescence lifetime (12 ns). The assignment of the lowest energy absorption transition to an intramolecular charge transfer (ICT) transition was confirmed by a protonation experiment (Figure 8): addition of 1 equiv of acid causes a large red shift ($\Delta\lambda = 134$ nm) of this band in accord with the formation of the strongly electron-withdrawing pyridinium fragment (Scheme 2). The monoprotonated form is not significantly emissive. A further addition of acid leads to the complete disappearance of the red color and a large shift of the absorption band to the blue, a behavior consistent with the subsequent protonation of the dibutylamino donor group under more acidic conditions, which leads to the inhibition of charge transfer ("pull−pull" compound).[25] This interpretation is corroborated by a profound blue shift of the emission from 518 to 416 nm ($\tau = 1.8$ ns) upon addition of an excess of acid. No significant variation of the absorption spectrum was observed with increasing solvent polarity (from toluene to dimethylformamide), in agreement with a weak ground-state dipole moment (μ_g) due to the distorted structure of the conjugated backbone ($\theta = 65°$). By contrast, the emission band shows a very strong positive solvatochromic shift (Table 3). The red shift in emission with increasing solvent polarity is accompanied by an increase

Table 3. UV−Visible and Emission Data of Terpyridine Derivatives

compd	solvent	λ_{max} (ϵ), nm (L·mol^{-1}·cm^{-1})	λ_{em} (nm)	ϕ (%)[c]	τ (ns)
L	CH_2Cl_2	361 (21800)− 376 (7500)[a]	518	26	12
	toluene	360[b]	412	12	
	THF	358[b]	555	26	
	DMF	357[b]	587	6.5	
	EtOH	365[b]	608	0.8	
	acetone	365[b]	612	5.5	
	CH_3CN	365[b]	629	2.3	
[LH][PF$_6$]	CH_2Cl_2	510 (3300), 396 (21000)	no		
[LH$_n$]^n+	CH_2Cl_2	399 (22500)	416	30	1.8

[a] Estimated with the deconvolution. [b] The ILCT transition is overlapped with the more intense transition and no shoulder is visible hindering any deconvolution. [c] Fluorescence quantum yields were measured using quinine sulfate in H_2SO_4 (1 M, aq) as the standard; $\phi = 0.546$.

(24) Sénéchal-David, K.; Toupet, L.; Maury, O.; Le Bozec, H. *Cryst. Growth Des.* **2006**, *6*, 1493−1496.

(25) For similar experiments on CT chromophores, see: (a) Maury, O.; Guégan, J.-P.; Renouard, T.; Hilton, A.; Dupau, P.; Sandon, N.; Toupet, L.; Le Bozec, H. *New J. Chem.* **2001**, 1553−1566. (b) Goodall, W.; Williams, J. A. G. *Chem. Commun.* **2001**, 2514−2515.

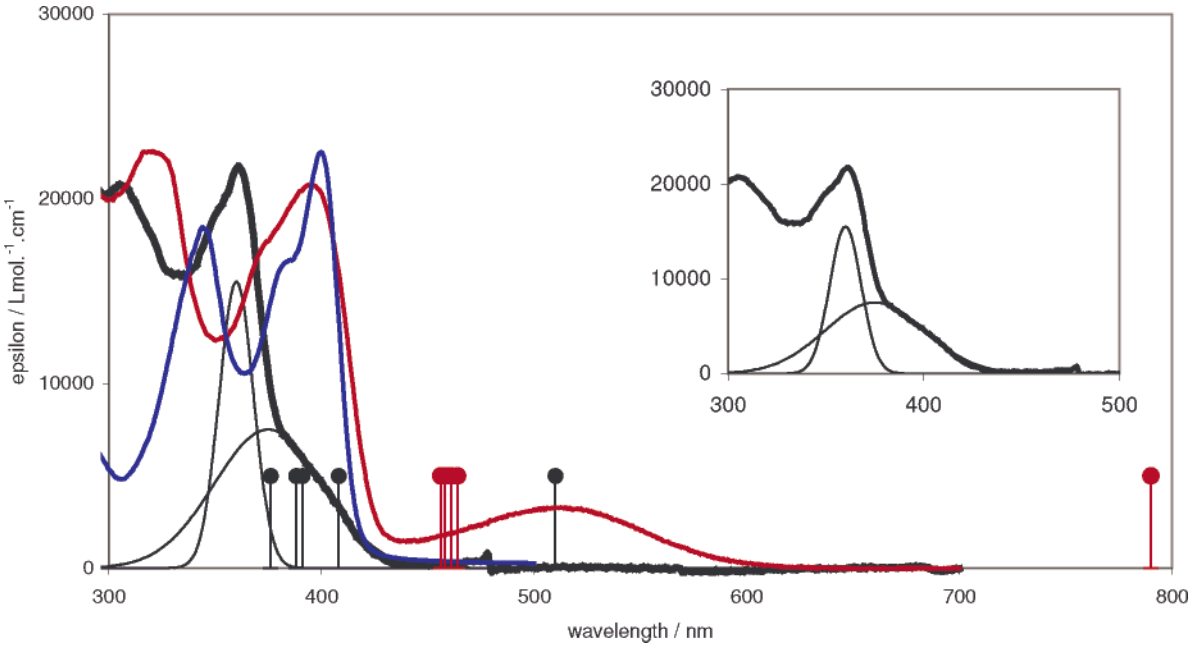

Figure 8. Absorption spectra of (i) **L** (black bold), deconvolution (inset), and simulation (black circle); (ii) the monoprotonated species $\mathbf{L}H^+$ (red and simulation in red circle); and (iii) the polyprotonated species (blue).

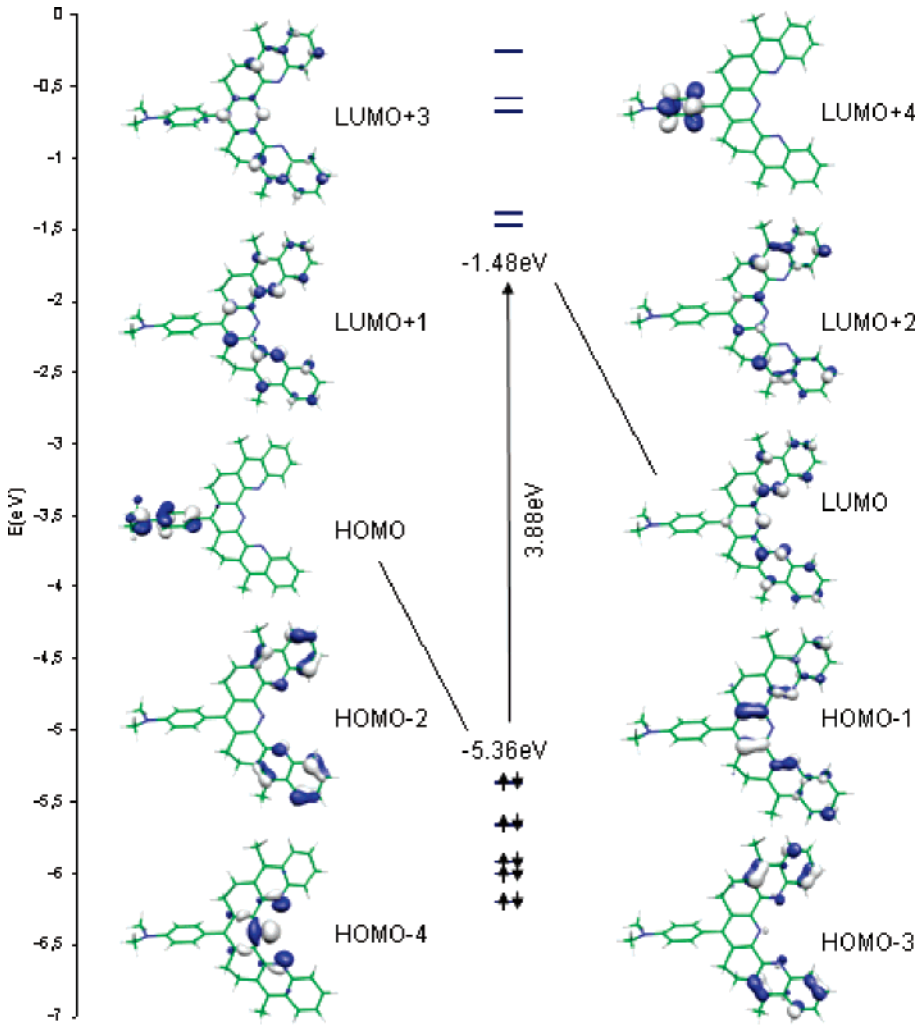

Figure 9. Molecular orbital energy diagram for **L′** (B3LYP/DZP).

of the Stokes shift and the bandwidth. This behavior is typical of charge-transfer character in the fluorescent excited state, featuring a large dipole moment (μ_e), and is quite similar to that described for nonannelated terpyridyl ligands.[26] Density

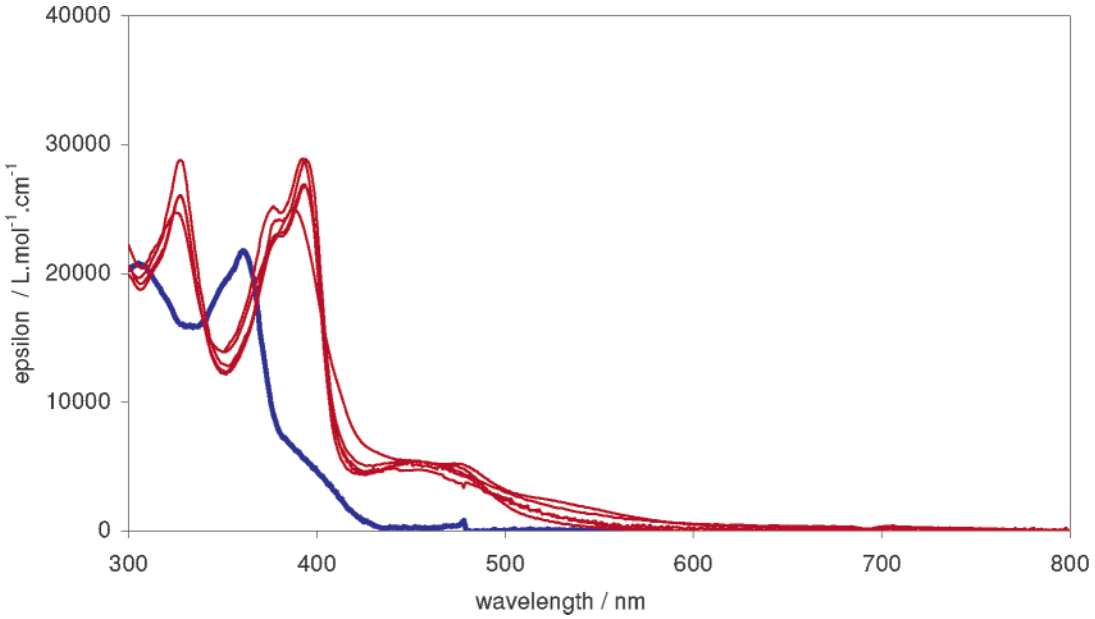

Figure 10. UV−visible absorption spectra of the ligand (blue), protonated species (violet), and Ln complexes (red).

functional theoretical (TDDFT) calculations were performed in order to understand these spectroscopic data. The molecular orbital energy diagrams of **L′** and **L′**H^+ are shown in Figures 9 and S4, respectively. The corresponding electronic transitions are listed in Table 4, and their energies are superimposed on the spectrum in Figure 8 (vertical lines). The lowest energy transition (exptl 376 nm, calcd 510 nm) involves almost exclusively (99%) the HOMO, localized on the donor part of the ligand, and the LUMO, delocalized on the three pyridinic rings (Figure 9). Thus, this transition can be classically described as an intramolecular charge transfer (ICT) transition. The second optical transition centered at 361 nm can be assigned to a "locally excited" state transition because it results from the overlap of four electronic excitations, each of them being a mixture of various HOMO(0 to −6) − LUMO(0 to +3) transitions (Table 4) featuring a main pyridinic $\pi-\pi^*$ character [(HOMO − 3, LUMO) or (HOMO − 6, LUMO)] with some minor ICT character (HOMO, LUMO + 2).

The photoinduced modifications of the electronic density distribution result in an important increase of the dipole moment in the Franck−Condon excited state. The effect of the (HOMO, LUMO) excitation on the geometries and the charge distributions has been studied using the CIS approach (configuration interaction with singles),[27] which starts from a Hartree−Fock (HF) description of the molecules. Although not very accurate regarding excitation energies, this method allows the determination of approximate wave functions and relaxed geometries of excited states. When the ground and the CIS excited states are compared, the following trends have been observed: (i) the magnitude of the dipole moment in the Franck−Condon excited state is roughly three times higher than that in the ground state; for instance, in the case of **L′**, it rises from 6.7 D (HF) to 18.1 D (CIS); (ii) the magnitude of this property diminishes in the geometry relaxed excited state; in the case of **L′**, its value is equal to 11.6 D, which remains much higher than the ground-state one; (iii) the θ angle in the geometry relaxed excited state is lower than in the ground state, thus indicating a more planar structure allowing a better π delocalization between the two parts of the molecules; for **L′**, this angle goes from ∼75° (HF ground state) to ∼50° (CIS excited state). Such relaxed ICT

Table 4. $f >$ 0.01 Lowest Excitations—DFT LB94/DZP Results

compd	transitions	energy λ (nm) (Δ*E* (eV))	oscillator strength (au)	composition	%
L′	1	510 (2.43)	0.041	HO→LU	99
	2	408 (3.04)	0.061	HO−3→LU	61
				HO−5→LU+1	26
	3	391 (3.17)	0.027	HO→LU+2	69
				HO−6→LU	21
	4	388 (3.20)	0.119	HO−6→LU	46
				HO→LU+2	30
				HO−3→LU	12
	5	376 (3.30)	0.101	HO→LU+3	74
				HO−3→LU+1	10
				HO−6→LU+1	9
L′H^+	1	790 (1.57)	0.229	HO→LU	98
	2	464 (2.67)	0.234	HO−3→LU	83
				HO→LU+3	8
	3	461 (2.69)	0.062	HO→LU+2	93
	4	458 (2.71)	0.018	HO→LU+3	69
				HO−5→LU	26
	5	456 (2.72)	0.022	HO−5→LU	72
				HO→LU+3	22
L′$Y(NO_3)_3$	1	667 (1.86)	0.069	HO→LU	99
	2	440 (2.82)	0.168	HO−3→LU	81
				HO−2→LU+1	6
				HO→LU+5	3
	3	431 (2.88)	0.015	HO−1→LU+1	64
				HO−3→LU+1	13
				HO−2→LU	12
	4	429 (2.89)	0.013	HO→LU+5	89
				HO−6→LU	4
	5	425 (2.92)	0.036	HO→LU+6	96
L′$Lu(NO_3)_3$	1	667 (1.86)	0.068	HO→LU	99
	2	441 (2.81)	0.169	HO−3→LU	82
				HO−2→LU+1	7
				HO−7→LU+1	3
	3	429 (2.89)	0.012	HO→LU+5	92
	4	425 (2.92)	0.034	HO→LU+6:	96

(26) (a) Goodall, W.; Wild, K.; Arm, K. J.; Williams, J. A. G. *J. Chem. Soc., Perkin Trans. 2* **2002**, 1660−1681. (b) Mutai, T.; Cheon, J.-D.; Tsuchiya, G.; Araki, K. *J. Chem. Soc., Perkin Trans. 2* **2002**, 862−865.
(27) Foresman, J. B.; Head-Gordon, M.; Pople, J. A.; Frisch, M. J. *J. Phys. Chem.* **1992**, *96*, 137.

Table 5. Linear and Nonlinear Optical Data for the Ligand and the Related Complexes

	λ_{iLCT} ($\lambda_{\pi-\pi^*}$) [nm][a]	ϵ [L·mol^{-1}·cm^{-1}]	$\nu_{1/2(ILCT)}$ [cm^{-1}]	f[b]	$\beta^{1.91}$ [c] [10^{-30} esu]	β_0 [d] [10^{-30} esu]
L	376 (361)	7500 (21800)	4294	0.14	190	155
[**L**H][PF_6]	510 (396)	7400 (22400)	3373	0.12	240	159
LY(NO_3)$_3$	454 (392)	4750 (28900)	5363	0.11	191	139
LLa(NO_3)$_3$	453 (391)	5400 (24500)	6055	0.14	186	136
LGd(NO_3)$_3$	452 (393)	5800 (26900)	4550	0.12	246	180
LDy(NO_3)$_3$	450 (394)	5400 (26700)	5825	0.14	260	190
LYb(NO_3)$_3$	452 (394)	5150 (28850)	5465	0.12	288	211

[a] Measured in dilute dichloromethane solution (1×10^{-5} mol·L^{-1}). [b] The oscillator strength is deduced from the UV−visible spectra according to $f = (4.319 \times 10^{-9})\epsilon\nu_{1/2}$. [c] Measured by HLS using $\lambda = 1.91$ μm as fundamental wavelength in concentrated dichloromethane solution (1×10^{-2} mol·L^{-1}). [d] Deduced from the two-level model.

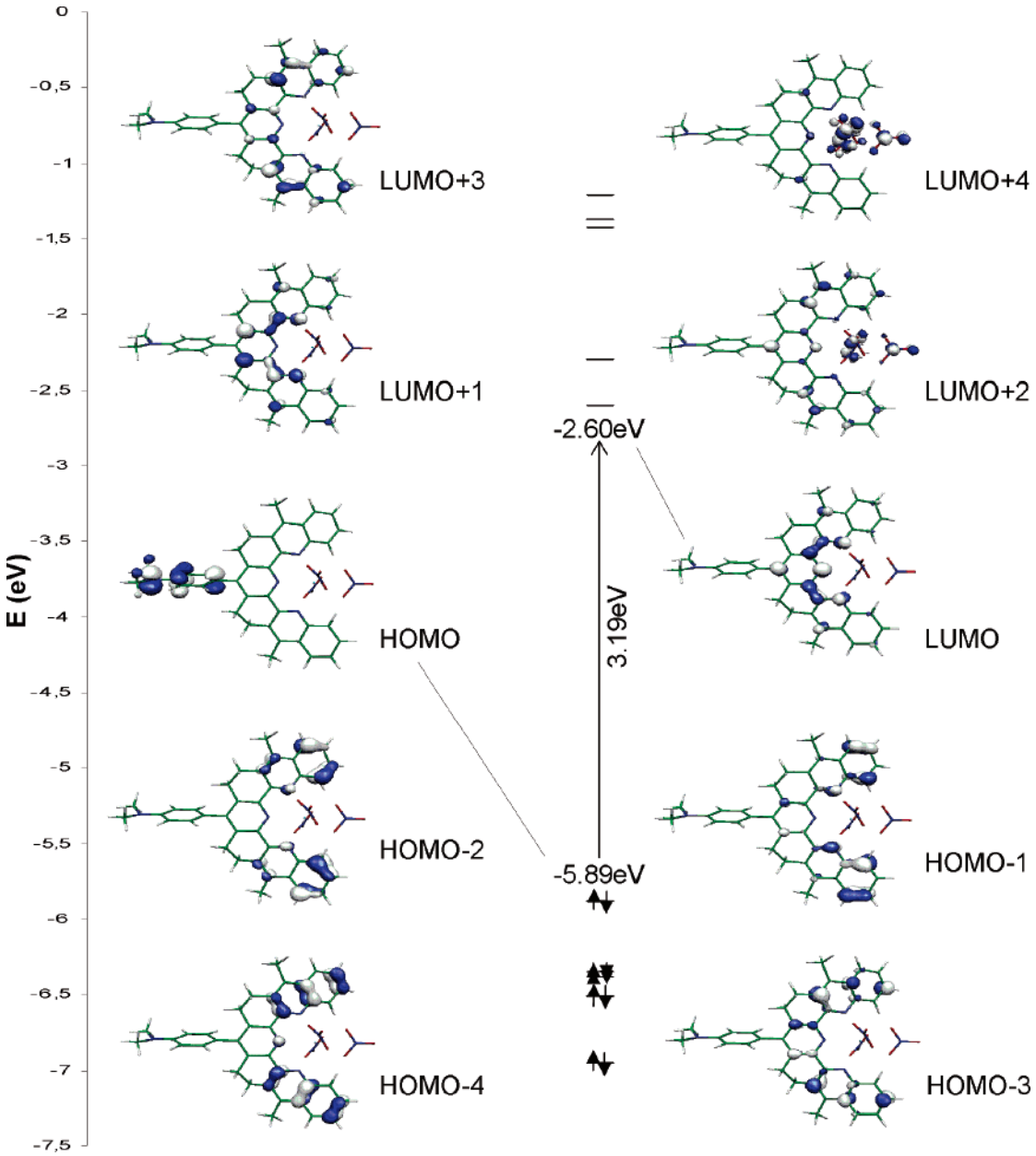

Figure 11. Molecular orbital energy diagram for **L′**Lu(NO_3)$_3$ (B3LYP/DZP).

state accompanied by a conformational change is generally referred to as twisted intramolecular charge transfer (TICT).[28] TICT states have already been described in the case of 4-dialkylaminophenylacridines[29] and are strongly sensitive to the solvent polarity and responsible for the solvent dependence

(28) For a review on TICT, see: Grabowski, Z. R.; Rotkiewicz, K.; Rettig, W. *Chem. Rev.* **2003**, *103*, 3899−4031.

(29) Herbich, J.; Kapturkiewicz, A. *J. Am. Chem. Soc.* **1998**, *120*, 1014−1029.

of the fluorescence quantum yield and of the Stokes shift. A more polar solvent contributes to a higher stabilization of the excited-state resulting in a red shift of the emission band and a decrease of the quantum yield.

B. Optical Properties and DFT Calculations of Lanthanide Complexes. All lanthanide ions behave similarly in terms of absorption spectra (Figure 10): the TICT transition is bathochromically shifted by ca. 75 nm upon complexation, the Lewis acidity of Ln^{3+} enhancing the acceptor strength of the terpyridyl moieties. It is also important to note that the oscillator strength of the TICT band (Table 5) is the same for all complexes (0.11−0.14) and similar to that of the ligand (0.14), the lower extinction coefficient ϵ of the complexes vs that of **L** being balanced by the broadening of the band. Interestingly, theoretical calculations performed in the cases of lutetium and yttrium unambiguously confirm (i) the CT character of the lowest energy transition with a 99% contribution of the HOMO−LUMO transition (Table 4 and Figure 11), (ii) the strong bathochromic shift induced by complexation, and (iii) identical behavior for both metals. This similar "ionochromic" effect has already been described previously on bipyridyl metal lanthanide complexes[30] and thus seems to be a general tendency of f-block elements.[13]

C. NLO Properties. The molecular second-order NLO properties were measured in solution by means of a harmonic light scattering technique (HLS) with an incident laser beam at 1.91 μm to avoid any two-photon induced fluorescence contribution to the second harmonic, and the results are summarized in Table 5.[31] The terpyridyl ligand **L** has a remarkably high and unexpected static β_0 value (β_0(**L**) = 155 × 10^{-30} esu), comparable to that of the parent nonannelated 4′-dibutylaminophenyl-2,2′:6′,2″-terpyridine (β_0^{HLS} = 147 × 10^{-30} esu).[32,33] This high NLO activity is much larger than those of other push−pull polypyridine derivatives[10a,10c] featuring classical planar π-conjugated systems and can be related to the twisted π-electron system as recently reported by Marks and Ratner.[34] Protonation of **L** does not lead to an increase of the static β_0 value (β_0(**LH**$^+$) = 159 × 10^{-30} esu), the increase of the dynamic β value being compensated by the dispersion factor due to the large red shift of the maximum absorption wavelength (Table 5). Concerning the lanthanide complexes, it is worth noting that the NLO activity significantly depends on the nature of the lanthanide. Whereas the lanthanum complex has a β_0 value (β_0(La) = 136 × 10^{-30} esu) similar to that of the free ligand (and to that of the protonated ligand), the other lanthanide (Gd, Dy, Yb) complexes display a regular increase of their NLO activities along the f-block element series. Keeping in mind that all of these complexes are isostructural and show the same UV−visible absorption spectrum, these NLO enhancements cannot be explained on the simple basis of the two-level model[35] and strongly suggest the participation of the metallic center. As recently reported in the case of the octupolar $Ln(DPA)_3^{3-}$ series,[13] the NLO study of the corresponding yttrium complex is particularly useful to rationalize this "metal-induced" NLO enhancement effect. Yttrium presents strong chemical similarities to lanthanides, and its ionic radius (1.075 Å) is very close to that of dysprosium (1.083 Å).[36] On the other hand, yttrium is not an f-block element and therefore has a $4f^0$ electronic configuration like lanthanum. Experimentally, the hyperpolarizability coefficient of yttrium, β(Y) = 191 × 10^{-30} esu, is very similar to that of lanthanum (186 × 10^{-30} esu) and significantly lower than that of dysprosium (260 × 10^{-30} esu): the difference between β(Y) and β(Dy) is much larger than the experimental error estimated to ±15% (HLS at 1.91 μm). Once again, it appears that the NLO activity variation along the lanthanide series can be better correlated to the f configuration rather to the ionic radius (Figure 12). This new effect has now been established on the basis of HLS for two isostructural lanthanide series, a dipolar one, [**L**Ln$(NO_3)_3$], and an octupolar one, $Ln(DPA)_3$,[3] having completely different structures. Moreover, the measurements were performed with two different fundamental laser wavelengths (1.91 and 1.06 μm) in different solvents (CH_2Cl_2 and H_2O). Therefore, one can conclude from these two experiments that the direct contribution of f electrons to the hyperpolarizability seems to be a general property of f-block complexes.

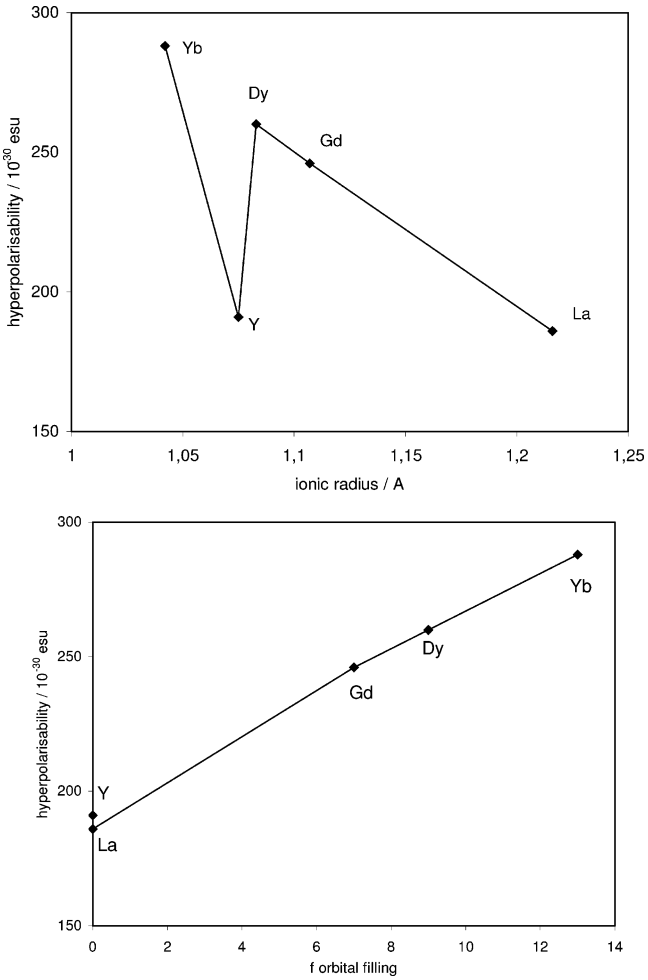

Figure 12. Plot of the hyperpolarizability coefficient ◆ vs ionic radius (top) and f orbital filling (bottom).

(30) Wang, B.; Wasielewski, M. R. *J. Am. Chem. Soc.* **1997**, *119*, 12−21.
(31) The detailed description of the experimental setup is described in: Le Bozec, H.; Le Bouder, T.; Maury, O.; Bondon, A.; Ledoux, I.; Deveau, S.; Zyss, J. *Adv. Mater.* **2001**, *13*, 1677−1681.
(32) Tancrez, N. Ph.D. Thesis, ENS−Cachan, France, 2005.
(33) The β_0^{EFISH} of this molecule was estimated to be 15 × 10^{-30} esu in ref 11g and in: Roberto, D.; Tessore, F.; Ugo, R.; Bruni, S.; Manfredi, A.; Quici, S. *Chem. Commun.* **2002**, 846−847.
(34) (a) Kang, H.; Facchetti, A.; Zhu, P.; Jiang, H.; Yang, Y.; Cariati, E.; Righetto, S.; Ugo, R.; Zuccaccia, C.; Macchioni, A.; Stern, C. L.; Liu, Z.; Ho, S.-T.; Marks, T. J. *Angew. Chem., Int. Ed.* **2005**, *44*, 7922−7925. (b) Keinana, S.; Zojerb, E.; Bredas, J.-L.; Ratner, M. A.; Marks, T. J. *J. Mol. Struct. (THEOCHEM)* **2003**, *633*, 227−235.
(35) Oudar, J. L. *J. Chem. Phys.* **1977**, *67*, 446.
(36) Shannon, R. D. *Acta Crystallogr., Sect. A* **1976**, *32*, 751−767.

Conclusion

In summary, a series of isostructural dipolar lanthanide(III) complexes featuring a functionalized terpyridine ligand have been synthesized, and the linear optical and nonlinear optical properties of the complexes and the ligand have been investigated. This study shows that coordination chemistry of lanthanide ions is a powerful tool for the design of efficient NLO-phores and that the molecular quadratic hyperpolarizability (β) values are strongly influenced by the nature of the lanthanide ion. A careful examination of the NLO measurements allows some conclusions to be drawn: (i) Concerning the ligand, the unexpected large β response could be attributed to the large dihedral angle between the donor and acceptor moieties leading to a twisted intramolecular charge transfer. (ii) Concerning the metal ions, the most striking result is the clear dependence of the first hyperpolarizability β on the lanthanide itself. A strong increase of β is observed on going from lanthanum to ytterbium, whereas for yttrium, which has no f electron like lanthanum, there is no evidence for significant increase of β. We propose that, as in the case of the octupolar series tris(dipicolinato)-lanthanates,[13] this enhancement can be better correlated to the f configuration rather than to the ionic radius. This intrinsic property of rare-earth metals is also particularly attractive in terms of transparency/nonlinearity tradeoff because improved β values are reached without any cost of transparency, and late lanthanide ions such as Er^{3+}, Tm^{3+}, Yb^{3+}, and Lu^{3+} appear to be very promising for the design of highly efficient NLO-phores because they are among the strongest Lewis acids of the periodic table and they feature a strong f electron density. This study opens the route for the design of multifunctional molecular materials combining lanthanide luminescence properties and NLO activity, which could be particularly interesting in the field of biological imaging.

Experimental Section

Computational Details. Our DFT geometry optimizations have been done employing the well-known functional B3LYP,[37] using a standard double-ζ polarized basis set, namely, the LANL2DZ supplemented by a single polarization function on heavy atoms. Another polarized double-ζ basis set, CEP-31G*, where core electrons of the heavier elements are also described by means of an effective core potential, has been used to treat the complexes, because LANL2DZ is not available for the metals under consideration. The CIS and DFT calculations were carried out using the Gaussian 03 package.[38] TDDFT[39] excitation energies calculations were performed using the Amsterdam Density Functional program (ADF2004.01)[40] and the PBE[41] as well as the LB94 functional.[42] The standard DZP basis set of ADF has been used for all atoms excluding hydrogen for which the DZ one has been employed. Note that the TDDFT excitation energy calculations (Table 4) have been carried out using the LB94 functional, whereas the displayed MO diagrams (Figure 13 and S3) are those of B3LYP. We checked that both functionals led qualitatively to the same energy ordering and compositions of the MOs under consideration. Molecular orbital plots were generated using the program MOLEKEL 4.3.[43]

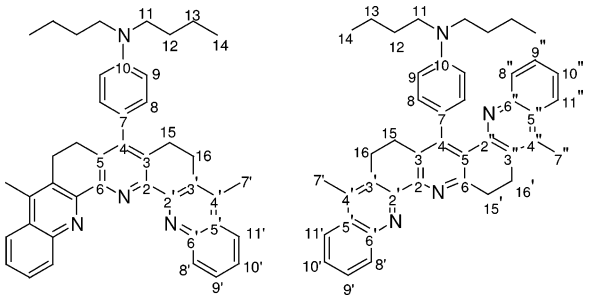

Figure 13. Atom numbering for **L** and **L-s**.

Crystal Structure Analysis. The sample was studied on a NONIUS Kappa CCD with graphite monochromatized Mo Kα radiation. The cell parameters are obtained with Denzo and Scalepack with 10 frames (psi rotation 1° per frame). The structure was solved with SIR-97,[44] which reveals the non-hydrogen atoms of structure. After anisotropic refinement, many hydrogen atoms may be found with a Fourier difference. The whole structure was refined with SHELXL97[45] by the full-matrix least-squares techniques (use of F magnitude; x, y, z, α_{ij} for C, N, and O atoms, x, y, z in riding mode for H atoms). ORTEP views were made with PLATON 98.[46] All the calculations were performed on a Silicon Graphics Indy computer. Crystallographic data for the structural analysis have been deposited with the Cambridge Crystallographic Data Centre, CCDC 229762 (Gd) and 222671 (Y).

HLS Measurements. Details concerning the experimental setup are described in ref 31.

Linear Absorption and Fluorescence Measurements. UV−visible spectra were recorded on a KONTRON UVIKON 941 spectrophotometer in diluted dichloromethane solution (ca. 10^{-5} mol·L^{-1}). Steady-state emission spectra were recorded in solution in 1 cm path length quartz cuvettes, using an Instruments S.A. Fluoromax equipped with a Hamamatsu R928 photomultiplier tube. Fluorescence quantum yields were measured by the method of continuous dilution using quinine sulfate as the standard ($\phi = 0.546$ in 1 M aqueous H_2SO_4,[47] correcting for the refractive index). The fluorescence lifetimes were measured using an Instruments S.A. Fluorolog Tau-3 instrument, by global fitting of the demodulation and phase shift of the emission, following excitation with sinusoidally modulated light over the frequency range 10−250 MHz. A suspension of Ludox in water was used as the standard, which acts a scattering sample of τ 0.0 ns.

General Procedures. All reactions were routinely performed under argon using Schlenk techniques. NMR spectra (^{1}H, ^{13}C, ^{31}P) were recorded at room temperature on BRUKER DPX 200, AC 300, or DMX500 spectrometers operating at 200.12, 300.13, and 500.13 MHz for ^{1}H, respectively. NMR data are listed in parts per million (ppm) and are reported relative to tetramethylsilane (^{1}H, ^{13}C), residual solvent peaks being used as internal standard (CD_2Cl_2 ^{1}H 5.25 ppm; ^{13}C 53.45 ppm). Complete attribution of the ^{1}H and ^{13}C spectra required 2D experiments (COSY, NOESY, H−C correlation (hmqc and hmbc

(37) Stephens, P. J.; Devlin, F. J.; Chabalowski, C. F.; Frisch, M. J. *J. Phys. Chem*. **1994**, *98*, 11623−11627.
(38) Frisch, M. J., et al. *Gaussian 03*, revision B.04, Gaussian, Inc.: Pittsburgh, PA, 2003.
(39) Van Gisbergen, S. J. A.; Snijders, J. G.; Baerends, E. J.; *Comput. Phys. Commun*. **1999**, *118*, 119.
(40) (a) Te Velde, G.; Bickelhaupt, F. M.; Van Gisbergen, S. J. A.; Fonseca Guerra, C.; Baerends, E. J.; Snijders, J. G.; Ziegler, T. *J. Comput. Chem.* **2001**, *22*, 931−967. (b) Fonseca Guerra, C.; Snijders, J. G.; Te Velde, G.; Baerends, E. J. *Theor. Chem. Acc*. **1998**, *99*, 391. (c) ADF2004.01, SCM, Theoretical Chemistry, Vrije Universiteit, Amsterdam, The Netherlands, http://www.scm.com.
(41) (a) Ernzerhof, M.; Scuseria, G. E. *J. Chem. Phys*. **1999**, *110*, 5029−5036. (b) Adamo, C.; Barone, V. *J. Chem. Phys*. **1999**, *110*, 6158−6170. (c) Adamo, C.; Cossi, M.; Scalmani, G.; Barone, V. *Chem. Phys. Lett*. **1999**, *307*, 265−271. (d) Adamo, C.; Scuseria, G. E.; Barone, V. *J. Chem. Phys*. **1999**, *111*, 2889−2899.
(42) Van Leeuwen, R.; Baerends, E. J. *Phys. Rev. A* **1994**, *49*, 2421−2431.
(43) Flükiger, P.; Lüthi, H. P.; Portmann, S.; Weber, J. *MOLEKEL 4.3*; Swiss Center for Scientific Computing: Manno, Switzerland, 2000; http://www.cscs.ch.
(44) Altomare, A.; Burla, M. C.; Camalli, M.; Carscarano, G.; Giacovazzo, C.; Guagliardi, A.; Moliterni, A. G. G.; Polidori, G.; Spagna, R. *J. Appl. Crystallogr*. **1998**, *31*, 74−77.
(45) Sheldrick, G. M. *SHELX93. Program for the Refinement of Crystal Structures*; University of Göttingen: Germany, 1993.
(46) Spek, A. L. *PLATON, A Multipurpose Crystallographic Tool*; Utrecht University: Utrecht, The Netherlands, 1998.
(47) Meech, S. R.; Phillips, D. J. *Photochemistry* **1983**, *23*, 193.

sequences)). High-resolution mass spectrometry measurements (FAB) were performed at the Centre Regional de Mesures Physiques de l'Ouest (Rennes, France) and elemental analysis by the Service Central d'Analyse du CNRS (Solaize, France). *N*,*N*-Dibutylaminobenzaldehyde was classically prepared by a Vilsmeier−Haack formylation. THF and diethyl ether were distilled over Na/benzophenone, DMF was distilled prior to use, and CH_2Cl_2 was distilled over CaH_2.

9-Methyl-1,2,3,4-tetrahydroacridine (1). In a round-bottom flask, cyclohexanone (6.1 mL, 58 mmol) was heated at 90 °C, and 2-aminoacetophenone hydrochloride (10 g; 58 mmol) was added by small fractions. The bottom flask was then equipped with a condenser, and the crude heterogeneous mixture was further heated overnight at 110 °C. After cooling to room temperature, the red-orange solid was dissolved in ethanol/HCl (12 N) [95/5 v/v]. The solution was then neutralized with an aqueous NaOH solution. Ethanol was evaporated, and the product extracted with diethyl ether (2 × 100 mL). The combined organic layers were washed with water (2 × 100 mL), dried over magnesium sulfate and filtered, and the solvent was removed under reduced pressure. The desired product was finally obtained as a brown-yellow solid (10.2 g, 89%). ^{1}H NMR (200.131 MHz; $CDCl_3$) $\delta_{(ppm)}$: 7.94 (dd, ^3J = 8.3 Hz and ^4J = 1.1 Hz, 1H), 7.87 (dd, ^3J = 8.3 Hz and ^4J = 1.3 Hz, 1H), 7.55 (ddd, ^3J = 8.3 Hz, ^3J = 8.3 Hz and ^4J = 1.3 Hz, 1H), 7.38 (ddd, ^3J = 8.3 Hz, ^3J = 8.3 Hz and ^4J = 1.1 Hz, 1H), 3.07 (t br, ^3J = 6.7 Hz, 2H), 2.79 (t br, ^3J = 6.1 Hz, 2H), 2.43 (s, 3H), 1.86 (m, 2 × 2H). ^{13}C NMR (50.332 MHz, $CDCl_3$) $\delta_{(ppm)}$: 157.8, 145.5, 140.6, 128.0, 126.4, 128.6, 127.6, 124.8, 122.9, 34.2, 26.5, 22.8, 22.4, 12.9. HRMS (EI) *m*/*z*: calcd for $[M]^+$ (found): 197.1204 (197.1198). Anal. Calcd for $C_{14}H_{15}N$ (found): C 85.24 (85.25); H 7.66 (7.72); N 7.10 (6.78).

***N*-Oxide-9-methyl-1,2,3,4-tetrahydroacridine (2).** A dichloromethane solution (300 mL) of 3-chloroperbenzoic acid (26 g, 105 mmol) was slowly added to a dichloromethane solution (100 mL) of **1** (10.2 g, 52 mmol) at 0 °C. The mixture was stirred for 4 h at room temperature and quenched with an aqueous NaOH solution. The organic layers were further washed with water (5 × 100 mL) and dried over $MgSO_4$, and the solvent was removed under reduced pressure giving **2** as a brownish solid. (10.83 g, 98%). ^{1}H NMR (200.131 MHz, $CDCl_3$) $\delta_{(ppm)}$: 8.77 (dd, ^3J = 8.5 Hz and ^4J = 1.2 Hz, 1H), 7.97 (dd, ^3J = 8.5 Hz and ^4J = 0.9 Hz, 1H), 7.70−7.50 (m, 2×1H), 3.19 (t, ^3J = 6.1 Hz, 2H), 2.85 (t, ^3J = 6.2 Hz, 2H), 2.51 (s, 3H), 1.88 (m, 2 × 2H). ^{13}C NMR (50.332 MHz, $CDCl_3$) $\delta_{(ppm)}$: 146.7, 139.1, 131.6, 129.9, 127.7, 129.0, 127.3, 123.9, 119.6, 27.1, 26.6, 22.0, 21.4, 13.4. HRMS (EI) calcd for $[M]^+$ (found): 213.1154 (213.1159).

9-Methyl-1,2,3,4-tetrahydroacridin-4-ol (3). In a two-neck round-bottom flask equipped with a reflux condenser, *N*-oxide-9-methyl-1,2,3,4-tetrahydroacridine (11,2 g, 52 mmol) was dissolved in dichloromethane (250 mL). Trifluoroacetic anhydride (17 mL, 120 mmol) was slowly added at room temperature (the reaction is exothermic). The solution was stirred for 5 h, and the solvent was evaporated. The crude solid was dissolved in methanol (50 mL) and saponified by an aqueous K_2CO_3 solution (2 M, 150 mL); a brown solid precipitated. The methanol was removed under reduced pressure, and the product was extracted with dichloromethane (2 × 150 mL). The combined organic layers were washed with brine (2 × 50 mL), dried over magnesium sulfate, and evaporated to dryness. The desired product was recovered as a brown solid (9.4 g, 84%). Note that this compound underwent spontaneous oxidation into the coresponding ketone. ^{1}H NMR (200.131 MHz, $CDCl_3$) $\delta_{(ppm)}$: 7.96 (d, ^3J = 8.3 Hz, 1H), 7.91 (d, ^3J = 8.4 Hz, 1H), 7.58 (dd, ^3J = 8.3 Hz and ^3J = 8.1 Hz, 1H), 7.45 (dd, ^3J = 8.1 Hz and ^3J = 8.4 Hz, 1H), 4.95 (s br, 1H), 4.76 (dd, ^3J = 10.3 Hz and ^3J = 10.0 Hz, 1H), 2.89 (m, 2H), 2.54 (s, 3H), 2.40−1.92 (2×m, 2×1H), 1.82 (m, 2H). ^{13}C NMR (50.332 MHz, $CDCl_3$) $\delta_{(ppm)}$: 159.2, 145.3, 142.0, 127.7, 127.3, 129.2, 128.5, 126.0, 123.5, 70.2, 30.3, 26.7, 19.6, 13.8. HRMS (EI) calcd for $[M]^+$ (found): 213.1153 (213.1154).

9-Methyl-2,3-dihydro-1*H*-acridin-4-one (4). To a dichloromethane solution (300 mL) of **5** (9.4 g, 44 mmol) was added MnO_2 (23 g, 264 mmol) at room temperature, and the heterogeneous solution was allowed to stir for 2 days. After filtration over Celite, the solvent was evaporated. The crude dark solid was purified by column chromatography (neutral alumina, dichloromethane as eluant). After evaporation of the solvent, the desired product was recovered as a brownish solid (5.41 g, 58%). ^{1}H NMR (200.131 MHz, $CDCl_3$) $\delta_{(ppm)}$: 8.31 (dd, ^3J = 8.1 Hz and ^4J = 0.8 Hz, 1H), 7.94 (dd, ^3J = 8.0 Hz and ^4J = 1.4 Hz, 1H), 7.67−7.51 (m, 2H), 3.08 (t, ^3J = 6.1 Hz, 2H), 2.82 (t, ^3J = 6.4 Hz, 2H), 2.60 (s, 3H), 2.22 (m, 2H). ^{13}C NMR (50.332 MHz, $CDCl_3$) $\delta_{(ppm)}$: 198.2, 148.4, 146.9, 143.6, 134.1, 129.4, 132.4, 129.6, 128.9, 123.8, 40.2, 27.2, 22.4, 14.5. HRMS (EI) *m*/*z* calcd for $[M]^+$ (found): 211.0997 (211.0989). Anal. Calcd for $C_{14}H_{13}NO$ (found): C 79.59 (79.72); H 6.20 (6.28); N 6.63 (6.10).

4-(4-Dibutylamino-benzylidene)-morpholin-4-ium Chloride (5). The product was prepared according to ref 18. In a Schlenk flask, *N*,*N*-dibutylaminobenzaldehyde (5 g, 21 mmol) was dissolved in diethyl ether (5 mL), and this solution was slowly added to a diethyl ether (5 mL) solution of trimethylsilyl chloride (2.97 g, 28 mmol) and silylated morpholine (4.44 g, 28 mmol). The solution was further stirred under reflux for 72 h, and a yellow precipitate was formed. After cooling to room temperature, the precipitate was filtered off under argon, and the solid was thoroughly washed with diethyl ether (3 × 25 mL). After removal of residual solvent under reduced pressure, the desired product was recovered as a yellow solid, very sensitive to air and moisture (5.08 g, 70%). ^{1}H NMR (200.131 MHz, $CDCl_3$) $\delta_{(ppm)}$: 8.42 (s, 1H), 7.79 (d, ^3J = 9.3 Hz, 2H), 6.89 (d, ^3J = 9,3 Hz, 2H), 3.88 (m, 4H), 3.49 (t, ^3J = 7.6 Hz, 4H), 3.22 (m, 4H), 1.58 (m, 4H), 1.35 (m, 4H), 0.96 (t, ^3J = 7.2 Hz, 6H).

Ligand L. In a Schlenk flask equipped with a condenser, 9-methyl-2,3-dihydro-1*H*-acridin-4-one (0.91 g, 4.3 mmol), 4-(4-dibutylamino-benzylidene)-morpholin-4-ium chloride **5** (0.73 g, 2.15 mmol), and freshly sublimed ammonium acetate (1.62 g, 21 mmol) were solubilized in chloroform (40 mL). The brownish-yellow mixture was refluxed for 18 h. After cooling to room temperature, the solution was hydrolyzed with water (20 mL) and aqueous ammonia (25%, 1 mL) and further stirred for 4 h. The crude was extracted with dichloromethane (2 × 50 mL), the organic layer was washed with water, dried under $MgSO_4$, and filtered, and the solvents were removed under vacuum. The two *S*- and *U*- isomers were separated by column chromatography {alumina activity II, gradient elution from dichloromethane to dichloromethane/acetone v/v 95/5 (R_f = 0.1)}. The desired product (*U*-isomer) was obtained as a yellow microcrystalline powder (0.69 g, 52%). ^{1}H NMR (CD_2Cl_2) δ: 8.4 (d, ^3J = 8.1 Hz, 2H, $H^{8'}$), 8.1 (d, ^3J = 8.1 Hz, 2H, $H^{11'}$), 7.7 (ddd, 2H, $H^{9'}$), 7.6 (ddd, 2H, $H^{10'}$), 7.1 (d, ^3J = 8.5 Hz, 2H, H^8), 6.7 (d, ^3J = 8.5 Hz, 2H, H^9), 3.3 (t, ^3J = 7.7 Hz, 4H, H^{11}), 3.1 (m, 4H, H^{16}), 2.9 (m, 4H, H^{15}), 2.7 (s, 6H, $H^{7'}$), 1.6 (m, 4H, H^{12}), 1.4 (m, 4H, H^{13}), 0.9 (t, ^3J = 7.2 Hz, 6H, H^{14}). ^{13}C NMR (CD_2Cl_2) δ: 153.0 ($C^{2'}$), 151.0 (C^2,C^6), 148.7 (C^4), 148.2 (C^{10}), 147.1 ($C^{6'}$), 141.0 ($C^{4'}$), 135.33 (C^3), 130.3 (C^3,C^5 masked), 130.6 ($C^{8'}$), 130.4 (C^8), 129.1 ($C^{9'}$), 128.5 ($C^{5'}$), 126.9 ($C^{10'}$),124.1 ($C^{11'}$), 122.99 (C^7), 111.5 (C^9), 51.13 (C^{11}), 29.8 (C^{12}), 26.0 and 25.8 (C,^{15}C^{16}), 20.8 (C^{13}), 14.2 and 14.3 ($C^{7'}$,C^{14}). UV−visible (CH_2Cl_2): λ_{max} = 375 nm (overlap), λ = 361 nm (21700). HRMS [M^+] calcd for $C_{43}H_{44}N_4$ (found): 616.3566 (616.3576). Elemental analysis calcd for $C_{43}H_{44}N_4 \cdot 2H_2O$ (found): wt % C 79.00 (79.11); wt % H 7.52 (7.41); wt % N 8.21 (8.58).

L-s. ^{1}H NMR ($CDCl_3$) δ: 8.4 (d, ^3J = 7.7 Hz, 1H, $H^{8'}$), 8.2 (d, ^3J = 7.6 Hz, 1H, $H^{8''}$), 8.0 (m, 2H, $H^{11'}$ $H^{11''}$), 7.6 (d, ^3J = 8.7 Hz, 2H, H^8), 7.7−7.5 (m, 4H, $H^{9'}$ $H^{10'}$ $H^{9''}$ $H^{10''}$), 6.8 (d, ^3J = 8.7 Hz, 2H, H^9), 3.8 (tr, ^3J = 6.7, 2H, $H^{15'}$), 3.4 (t, ^3J = 7.5 Hz, 4H, H^{11}), 3.1 (m, 4H, H^{16} $H^{16'}$), 2.9 (m, 2H, H^{15}), 2.7 and 2.6 (s, 6H, $H^{7'}$ $H^{7''}$), 1.7 (m, 4H, H^{12}), 1.4 (m, 4H, H^{13}), 1.0 (t, ^3J = 7.2 Hz, 6H, H^{14}). ^{13}C NMR ($CDCl_3$) δ: 156.54, 153.07, 152.63, 151.16, 148.15, 147.10, 145.91, 141.11, 139.38, 139.04, 132.92, 131.68, 131.20, 131.02, 130.91, 130.34, 130.03, 128.35, 128.05, 128.00, 127.44, 126.94, 126.74, 126.19, 123.73, 123.37,

111.03, 50.86, 29.50, 27.15, 25.97 (two signals overlapped), 25.31, 20.42, 14.08 (two signals overlapped), 13.97. HRMS $[M + H]^+$ calcd for $C_{43}H_{45}N_4$ (found): 617.3644 (617.3650).

[LH][PF$_6$]. To an acetone solution (15 mL) of **L** (100 mg, 0.16 mmol) was slowly added 1 equiv of a diluted solution of HPF_6 in water (2.8 mL, 0.19 mmol) at room temperature. The initially yellow solution turned rapidly to deep red and was stirred at room temperature for 4 h. The solvent was then removed under vacuum; the resulting solid was dissolved in the minimum amount of dichloromethane and precipitated upon addition of pentane (50 mL). After filtration, the red solid was dried under vacuum (96.6 mg, 78%). ^{1}H NMR (CD_2Cl_2) δ: 8.3 (d, br, ^3J = 8.0 Hz, 2H, H$^{8'}$), 8.2 (d, ^3J = 8.0 Hz, 2H, H$^{11'}$), 7.8 (m, 4H, H$^{9',10'}$), 7.2 (d, ^3J = 8.8 Hz, 2H, H^8), 6.9 (d, ^3J = 8.8 Hz, 2H, H^9), 3.4 (t, ^3J = 7.6 Hz, 4H, H^{11}), 3.3 (m, 4H, H^{16}), 3.2 (m, 4H, H^{15}), 2.8 (s, 6H, H$^{7'}$), 1.7 (m, 4H, H^{12}), 1.5 (m, 4H, H^{13}), 1.0 (t, ^3J = 7.3 Hz, 6H, H^{14}). ^{31}P NMR (CD_2Cl_2) δ: −144.4 (hept, ^3J = 710 Hz). UV−visible (CH_2Cl_2): λ_{max} = 519 nm (9500), λ = 408 nm (25500). Elemental analysis calcd for $C_{43}H_{45}N_4PF_6 \cdot H_2O$ (found): wt % C 66.14 (65.93); wt % H 6.07 (6.04); wt % N 7.18 (7.10).

General Procedure for the Synthesis of LLn(NO$_3$)$_3$. In a Schlenk flask, $Ln(NO_3)_3 \cdot xH_2O$ (Ln = Y, La, Nd, Gd, x = 6; Ln = Dy, Yb, x = 5) was dissolved in dichloromethane (5−10 mL) at room temperature. A dichloromethane solution of ligand **L** was then added via a syringe, and the pale yellow mixture turned immediately to orange. After 1 h stirring at room temperature, the solvent was evaporated under vacuum. The resulting complex was then dissolved in the minimum amount of hot acetonitrile and purified by low-temperature crystallization (−20 °C). The microcrystalline powder was finally filtered off, dissolved with dichloromethane, and precipitated in pentane. After filtration and evaporation of the solvents, the desired complexes were recovered as orange powders. In the case of gadolinium and yttrium, the crystallization gave crystals suitable for X-ray diffraction analysis, whereas only very thin needles could be obtained in the case of lanthanum, dysprosium, and ytterbium.

LLa(NO$_3$)$_3$ ^{1}H NMR (CD_2Cl_2) δ: 8.5, (d br, 2H, H$^{8'}$), 8.1 (d br, 2H, H$^{11'}$) 7 (m br, 2 × 2H, H$^{9'}$,10′), 7.0 (d, ^3J = 8.5 Hz, 2H, H^8), 6.7 (d, ^3J = 8.5 Hz, 2H, H^9), 3.3 (t, ^3J = 7.5 Hz, 4H, H^{11}), 3.0 (m, 4H, H^{16}), 2.8 (m, 4H, H^{15}), 2.7 (s, 6H, H$^{7'}$), 1.6 (m, 4H, H^{12}), 1.4 (m, 4H, H^{13}), 1.0 (t, ^3J = 7.0 Hz, 6H, H^{14}). UV−visible (CH_2Cl_2): λ_{max} = 450 nm (5400), λ = 394 nm (26700). Elemental analysis calcd for $LaC_{43}H_{44}N_7O_9 \cdot CH_2Cl_2$ (found): wt % C 51.47 (50.18); wt % H 4.52 (4.67); wt % N: 9.55 (9.71).

For **L**Gd(NO$_3$)$_3$, no NMR measurements could be performed due to the strong paramagnetism of the metal: λ_{max} = 452 nm (5400), λ = 393 nm (26900). Elemental analysis calcd for $GdC_{43}H_{44}N_7O_9 \cdot CH_2Cl_2$ (found): wt % C 50.57 (51.38); wt % H 4.44 (4.86); wt % N 9.38 (9.38).

LDy(NO$_3$)$_3$ ^{1}H NMR (CD_2Cl_2) δ: 0.8, −64.11, −76.5, −95.4 (s, 4 × 2H, H$^{8',9',10',11'}$), −41.8 (s, 6H, H$^{7'}$), 33.6, −1.7 (s, 2 × 4H, H^{15,16}), 47.0, 24.7 (s, 2 × 2H, H^{8,9}), 12.1, 10.3, 8.0 (s, 3 × 4H, H^{11,12,13}), 6.22 (s, 6H, H^{14}). UV−visible (CH_2Cl_2): λ_{max} = 450 nm (5400), λ = 394 nm (26700). Elemental analysis calcd for $DyC_{43}H_{44}N_7O_9 \cdot CH_2Cl_2$ (found): wt % C 50.32 (50.18); wt % H 4.41 (4.70); wt % N 9.34 (9.71).

LYb(NO$_3$)$_3$ ^{1}H NMR (CD_2Cl_2) δ: 114.4, 27.3, 27.3, 23.6 (m, br, 4 × 2H, H$^{8',9',10',11'}$), 14.0 (s, 6H, H$^{7'}$), 2.9, −6.4 (s, br, 2 × 4H, H^{15,16}), 1.96, −4.0 (d, J = 8.7 Hz, 2 × 2H, H^{8,9}), 0.86, −0.4, −0.7 (s, 3×4H, H^{11,12,13}), −0.4 (s, 6H, H^{14}). UV−visible (CH_2Cl_2): λ_{max} = 452 nm (5150), λ = 394 nm (28850). Elemental analysis calcd for $YbC_{43}H_{44}N_7O_9 \cdot CH_2Cl_2$ (found): wt % C 49.82 (49.71); wt % H 4.37 (4.41); wt % N 9.24 (9.82).

LY(NO$_3$)$_3$ ^{1}H NMR (CD_2Cl_2) δ: 8.3 (d, ^3J = 8.5 Hz, 2H, H$^{8'}$), 8.1 (d, ^3J = 8.1 Hz, 2H, H$^{11'}$), 7.8 (dd, 2H, H$^{9'}$), 7.7 (dd, 2H, H$^{10'}$), 7.0 (d, ^3J = 8.8 Hz, 2H, H^8), 6.7 (d, ^3J = 8.8 Hz, 2H, H^9), 3.3 (t, ^3J = 7.5 Hz, 4H, H^{11}), 3.2 (m, 4H, H^{16}), 2.9 (m, 4H, H^{15}), 2.7 (s, 6H, H$^{7'}$), 1.6 (m, 4H, H^{12}), 1.4 (m, 4H, H^{13}), 0.9 (t, ^3J = 7.0 Hz, 6H, H^{14}). λ_{max} = 454 nm (4750), λ = 392 nm (28900). Elemental analysis calcd for $YC_{43}H_{44}N_7O_9$ (found): wt % C 57.92 (58.17); wt % H 4.97 (5.15); wt % N 10.99 (10.40).

Supporting Information Available: Crystallographic packing of [Gd**L**^{1}(NO$_3$)$_3$·CH$_3$CN], selected crystallographic data and collection parameters for gadolinium and yttrium complexes, crystallographic data in CIF files, optimized geometry of yttrium complex, solvatochromism in the emission of **L** at room temperature, molecular orbital energy diagram for **L**′H$^+$, and complete ref 38. This material is available free of charge via the Internet at http://pubs.acs.org.

JA063586J